

Simulation of Gradient Coil Induced Eddy Currents and Their Effects in a Head-Only HTS MRI Magnet

Michael Poole, Hector Sanchez Lopez, Osamu Ozaki, Hitoshi Kitaguchi, Iwao Nakajima, Shin-ichi Urayama, Ken-ichi Sato, Hidenao Fukuyama and Stuart Crozier,

Abstract—In this work we simulate the effects of eddy currents induced by switched gradient coils in the cylindrical cryostat structures of a HTS MRI magnet. A novel network method was used with spectral decomposition of the current density in the ϕ and z directions to simulate the effects of X gradient coils. Two types of active magnetic shielding were simulated and it was found that one type is able to reduce the power of the eddy currents in the cryostat to a greater extent than the other. These results will inform the design of gradient coils that protect the HTS magnet from eddy current induced heating and vibrations.

Index Terms—MRI, Gradient Coils, Eddy current, HTS, Network Method.

I. INTRODUCTION

MAGNETIC resonance imaging (MRI) is one of the most common applications of superconductivity. A highly-uniform, intense magnetic field is generated by a superconducting magnet, most commonly made of the niobium-titanium (NbTi) wire, immersed in liquid helium at 4.2K or less. High-temperature superconducting (HTS) magnets that can operate without liquid helium are an attractive prospect indeed. Development of this new generation of HTS magnets for MRI requires careful consideration in the design and engineering of the other parts of the MRI scanner. Of particular concern is the interaction between the gradient coils and the magnet. This interaction is simulated in the present study to assess ways to minimise the potentially harmful effect of the gradient coils on a HTS magnet.

Gradient coils [1] are arrangements of wire placed inside the room-temperature bore of the MRI magnet that are designed to conduct currents over 600 Ampères switched at kHz. Their presence is essential for MRI because they generate the magnetic fields that manipulate the nuclear spins in such a way that images can be created from nuclear magnetic resonance (NMR) signals [2], [3]. The high current and fast switching in the gradient coil is desired for fast imaging. The magnetic fields generated by the gradient coils vary

linearly in the region of interest (ROI) but extend out to the cryostat of the superconducting magnet. In accordance with Faraday's law these changing magnetic fields induce an electromotive force (EMF) within the conducting layers of the cryostat which generates eddy currents (also known as Foucault currents). These eddy currents cause many deleterious effects in MRI; resistive dissipation of eddy currents results in Ohmic heating, Lorentz forces cause mechanical vibration and secondary magnet fields are generated which severely disturbs the imaging.

Some standard methods exist to prevent the generation of eddy currents and to counteract their effects. Passive shielding provides a highly conducting surface interposed between the gradient coil and the magnet cryostat [4]. Eddy currents are generated in the passive shield and the magnitude of eddy currents reaching in the cryostat is reduced. This transfers some of the Ohmic heating and vibration from the cryostat, in which the superconducting wires reside, to the passive shield where active cooling and vibration damping may be applied more easily. The temporally-varying secondary magnetic field from the eddy currents remains.

The secondary field is smaller than, and opposite in sign to, the linearly varying gradient field and it decays exponentially with some characteristic time-constant(s). A technique known as pre-emphasis [5], [6] attempts to counteract the secondary magnetic field by adding extra current during switching with the same time constant(s) and opposite sign to the secondary field. A filter can be designed to modify the waveform of electric current in the gradient coil which results in the restoration of the desired temporal behaviour of the magnetic field in the ROI. This approach alone does not address the problems of Ohmic heating and vibration in the cryostat, and in fact increases them somewhat due to the temporarily increased current.

Active shielding [7] was proposed in which an additional coil is interposed between the primary gradient coil wires and the cryostat. A linearly-varying field is still generated in the ROI, but is close to zero outside and at the cryostat vessel. This greatly reduced magnetic field causes a large reduction in the induced eddy current magnitude and therefore addresses Ohmic heating, vibration and the secondary magnetic field effects on imaging.

Several variants of the methods mentioned above have been presented and it is common to find them used in conjunction in commercial MRI scanners. It is possible to design gradient coils with active shielding to optimally deal with the secondary field effects [8] or Ohmic heating and vibration effects [9].

M. Poole, H. Sanchez Lopez and S. Crozier are with the School of Information Technology and Electrical Engineering, University of Queensland, Brisbane, QLD, 4072, Australia. e-mail: michael@itee.uq.edu.au.

O. Ozaki is with Kobe Steel Ltd., Kobe 651-2271, Japan.

H. Kitaguchi is with the Superconducting Materials Center, National Institute for Material Science (NIMS), Tsukuba 305-0047, Japan.

I. Nakajima is with Takashima Seisakusho Co Ltd., Tokyo, Japan

S. Urayama and H. Fukuyama are with the Human Brain Research Centre (HBRC), Kyoto University Graduate School of Medicine, Kyoto, 606-8507, Japan

K. Sato is with Sumitomo Electric Industries Ltd., Osaka, 554-0024, Japan

Manuscript received February 17, 2011

In the present study the design of gradient coils for an experimental HTS magnet system was considered and so Ohmic heating and vibration in the cryostat are more of a concern than the secondary magnetic field. The differences between the two approaches are studied by simulation with respect to measures of gradient and shielding performance.

A network method was recently developed [10] that is capable of efficiently simulating the eddy current in finite-length, multi-layered, thick cylinders that are generated by any gradient coil; X, Y and Z. This method presented an improvement over previous network methods that were only able to simulate Z gradient coils [11], [12]. The total power of the eddy currents induced in each cryostat layer can be calculated, which directly relates to the heat energy deposited per second and is thought to be closely related to the power of mechanical vibration and hence noise [13]. Through Fourier-Bessel relations [14], the magnetic field produced by the eddy currents is computed. Eddy current simulations can be time-harmonic or transient.

Gradient coils are designed using different shielding approaches, simulated with the network method and compared to find suitable coils that protect the magnet as much as possible.

II. METHODS

A. Geometric and Electromagnetic Problem Definition

A cross-section drawing is shown in Fig. 1 of the principal structures of the HTS MRI system for the purposes of eddy current simulation; it is a vertical bore system for human head imaging. The region of interest (ROI) is centred at the origin and is an oblate spheroid with major and minor diameters of 250 and 200 mm respectively. The gradient coil set (includes the gradient coil, shim coils and associated cooling mechanism) is shown by shaded boxes surrounding the ROI. It is asymmetrically positioned about the origin with each coil extending 180 mm downwards and 410 mm upwards. The inside and outside diameters (ID and OD) of the complete gradient coil set are 350 and 494 mm respectively. The magnet housing consists of the “warm bore” (WB), “cold shield” (CS) and “bobbin” (BN) for the purposes of the electromagnetic simulation; the geometric and electromagnetic properties of which are give in Table I. The magnet wires are shown (as boxes with crosses inside) but are not part of the eddy current simulation. Also, as part of the CS, there will be about 20 layers of approximately $0.06 \mu\text{m}$ Aluminium “supershielding” which are assumed to be magnetically transparent and not included in the simulation. A frequency of 1 kHz is assumed for any time-harmonic simulation unless otherwise stated.

B. Network Method for Eddy Current Simulation

To simulate the three-dimensional (3D) eddy currents that occur in the WB, CS and BN, we use a recently proposed network method [10]. Finite element simulations are not feasible since an elementary calculation of the approximate number of mesh elements required to accurately simulate the cold shield alone with a resolution of 0.6 mm would be approximately 15,000,000. Furthermore, since this is a boundary element method (BEM) we need not mesh the air

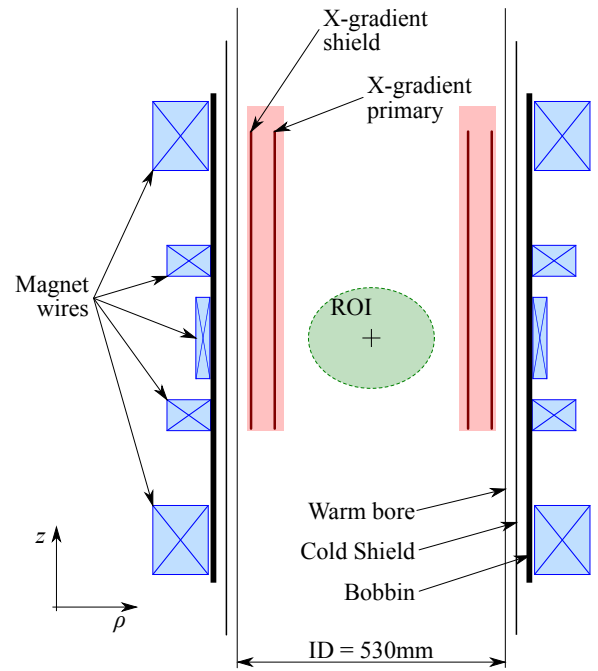


Fig. 1. Cross-sectional scale drawing of the HTS magnet and gradient coil structures. The region of interest (ROI), gradient coil unit, X-gradient primary and shield layer, warm bore, cold shield, bobbin and magnet wires are shown.

TABLE I
GEOMETRIC AND ELECTROMAGNETIC PROPERTIES OF THE HTS MAGNET CRYOSTAT AND SUPPORT STRUCTURE

Layer number	1	2	3
Layer name	Warm bore	Cold shield	Bobbin
Length (mm)	1310	1179	972
ID (mm)	530	573	616
Thickness (mm)	2.0	3.0	11.45
Material	Stainless Steel	Brass	Stainless Steel
Temperature (K)	300	80	20
ρ ($\mu\Omega\text{m}$)	0.62	0.0432	0.40
δ (mm)	12.5	3.3	10.1
N_s	1	5	6

between the conducting structures. The method works by subdividing the thick, conducting cylinders into sub-layers. On each sub-layer the eddy currents are approximated as a finite number of truncated, sinusoidal functions of the type originally used in the design of gradient coils [15], [16]. The expressions for the inductive coupling between each of these basis function (and themselves), as well as their power dissipation, is well known and makes use of the Fourier-Bessel expansion of the Green’s function in cylindrical coordinates [14]. The gradient coil is modelled as a set of short, infinitely-thin wire elements that may carry a time-harmonic or arbitrary transient waveform current to excite the electromagnetic system.

This method obtains the current density of each sub-layer in the system. From this wealth of information it is possible to calculate useful parameters which relate to some objective measure of the efficacy of shielding. In this paper we use the total power in each layer which gives a measure of the amount of heat generated as well as some indication of

the vibrational power imparted to each layer [13]. The peak current density may also be of interest as it relates to the maximum local Lorentz force experienced by the cryostat. Also of use are measures of the maximum magnetic field and the average gradient field generated in the ROI caused by the eddy currents.

C. Selection of the Simulation Parameters

Before studying different gradient coils we need to decide upon some parameters for the network method simulation. The choice of parameters should provide a trade-off between calculation accuracy and computational time. In the ϕ direction the eddy currents are modelled as a sum of $\cos(m\phi)$ basis functions for $m = 0, 1, 2, \dots, M$. In the case of the X gradient coils studied here we can assume that $m = 1$.

1) *Sub-layers*: The network method separates each thick cylindrical layer into a number of sub-layers. Each sub-layer is then considered as infinitely thin. There needs to be enough layers to accurately represent the skin-depth of the eddy current in each surface. The gradient coil shown in Fig. 2 a) was used to drive the system. The number of sub-layers was chosen so that their thickness was less than $1/5^{\text{th}}$ of the skin depth in each layer (see Table I) resulting in 1, 5 and 6 layers for WB, CS and BN respectively. Representing the thick cylinders as a finite number of sub-layers necessarily introduces some small error that decreases with decreasing sub-layer thickness. To estimate this error the number of sub-layers was doubled (to 2, 10 and 12) and the total power dissipation in the WB was compared.

2) *Number of Basis Functions*: The electric and magnetic field possess mainly low spatial frequencies in ϕ and z directions at the warm bore and cold shield. Increasing the number (and therefore maximum spatial frequency) of the basis functions will model the eddy currents with increasing accuracy. Enough basis functions are chosen to produce approximately the same error as the number of sub-layers does. Again, the total power dissipation in the WB was calculated for increasing numbers of basis functions until a low enough error was reached.

D. Gradient Coil Design

The geometry of the system is axisymmetric and therefore we use an axisymmetric inverse boundary element method (BEM) [17], [18] to design the gradient coils. Alternatively, asymmetric sum-of-sinusoids [19], [20]) or triangular boundary element [21], [22] methods could have been used.

Many properties of the gradient coil can be optimised in the design process and improving one property usually means that other properties of the coil become worse. This trade-off is governed by an optimisation functional, $U(\psi_C)$, that contains each of the properties of the gradient coil that are of concern. The optimisation functional that was minimised in this work is given in Eq. 1 as a function of the free parameters of the values of the stream function at each node on the gradient coil surface, ψ_C .

$$U(\psi_C) = f(\psi_C) + \alpha e(\psi_C) + \beta P(\psi_C) - \sum_{p=x,y} \lambda_p T_p(\psi_C), \quad (1)$$

where $f(\psi_C)$ is the field error in the ROI, $e(\psi_C)$ is the shielding term, $P(\psi_C)$ is the power dissipation of the gradient coil and $T_p(\psi_C)$ is the p^{th} torque value. α and β are user-defined trade-off parameters that control the coil design, and λ_p are Lagrange multipliers used to ensure torque-balancing. p may reflect either the x or y component of the torque.

Within the method described above there are two principal ways to enforce the active shielding of a gradient coil. Gradient coils are designed with both approaches and simulated with the network method. Only one cryostat surface can be accurately modelled with the inverse BEM to enforce the shielding which was selected to be the cold-shield.

1) *Minimal Eddy Field (MEF) Shielding*: The first aims to minimise sum-of-squares of the secondary magnetic field in the ROI. This can be written

$$e(\psi_C) = \sum_k [B_{Ez}(\mathbf{r}_k, \psi_C)]^2, \quad \mathbf{r}_k \in \text{ROI}, \quad (2)$$

where $B_{Ez}(\mathbf{r}_k, \psi_C)$ denotes the z component of the magnetic field due to the eddy currents at the point \mathbf{r}_k from a gradient coil defined by ψ_C . A linear relationship between the induced currents in the cryostat and the currents in the gradient coil can be defined through their stream-functions ψ_E and ψ_C respectively and a mutual coupling that either assumes a step change in time or a time-harmonic change of ψ_C [8].

2) *Minimal Eddy Power (MEP) Shielding*: The second way of enforcing the active shielding is to minimise the power of the eddy currents in the cryostat by

$$e(\psi_C) = P_E(\psi_E). \quad (3)$$

III. RESULTS

A. Gradient Coils

Two actively-shielded, X gradient coils were designed for the MR system described above; one with MEP and the other with MEF shielding. The wire patterns of the primary and shield coils are shown in Fig. 2 and their relevant coil properties are given in Table II. Figure 2 shows the position of the centres of the wires for one half of each coil unwrapped from its cylindrical shape onto a flat plane.

TABLE II
GRADIENT COIL PORPRTIES

Shielding type	MEF	MEP
Number of contours of ψ_C	8	7
Current for 10 mTm^{-1} (A)	223.7	279.3
Min wire gap (mm)	11.0	11.1
Inductance (μH)	23.6	17.9

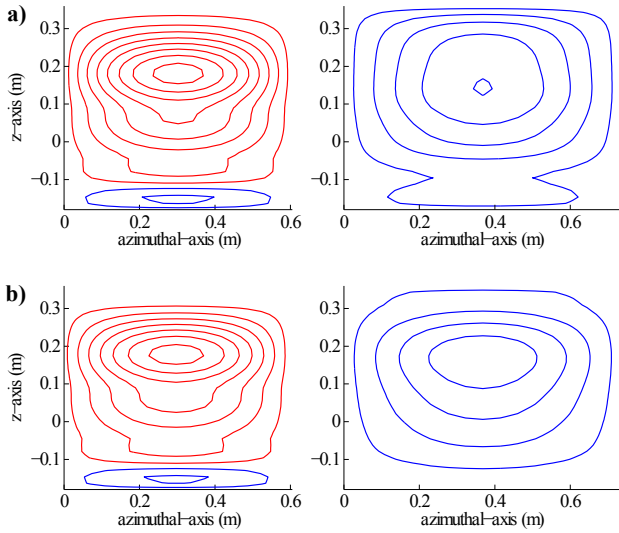


Fig. 2. The wire pattern for the X-gradient coils used in this simulation designed with a) MEF and b) MEP. The primary coils are shown on the left and their shields on the right. Red wires indicate reversed current with respect to blue.

B. Selection of the Simulation Parameters

1) *Sub-layers*: The total power deposited in the each layer of the cryostat was simulated for 1, 5 and 6 sub-layers in the WB, CS and BN. The difference between the power dissipation in the WB compared to 2, 10 and 12 layers was 0.7%.

2) *Number of Basis Functions*: The number of sinusoidal basis functions per sub-layer was increased from 4 to 30 and the resulting power dissipation in each layer is plotted in Fig. 3 as well as the asymptotic power dissipation value (based on an exponential fit). The number of basis functions required to produce less than 1% error with respect to the asymptotic value was 28.

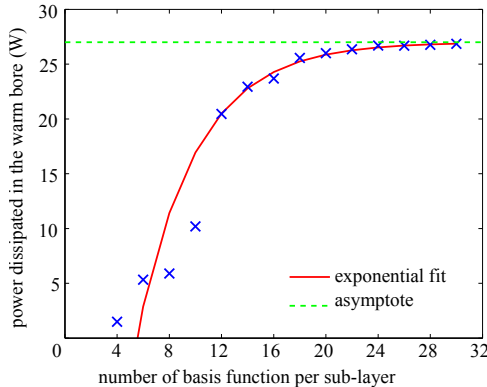


Fig. 3. Variation of the power dissipated in the WB as the number of basis functions used in z . A gradient field of 10 mTm^{-1} was used at 1 kHz.

With 28 sinusoidal basis function in z (14 sine and 14 cosine), 1 in ϕ and $1 + 5 + 6 = 12$ sub-layers the eddy current simulation had a total of 336 basis functions.

C. Simulation Results of HTS System

1) *Eddy Currents*: The simulation yields the stream function of the eddy current densities on each sub-layer of the

system. These data were reconstructed to obtain the eddy currents which are a complex-valued, three-dimensional vector field. There is a considerable amount of information which we represent here by showing J_ϕ in the ρ and z directions at $\phi = 0$. $J_\rho := 0$ by the network method and J_z can be derived from J_ϕ and $\nabla \cdot \mathbf{J} = 0$. All current density data presented possess $\cos \phi$ behaviour. Figure 4 shows the eddy current density behaviour through the thickness (ρ -dimension) of the three cylindrical layers of the magnet cryostat and support structures. The root-mean-squared (RMS) value of the current density was calculated by summation in each sub-layer in the z -direction. Data from both coils (MEF and MEP) are shown on the same graph for comparison.

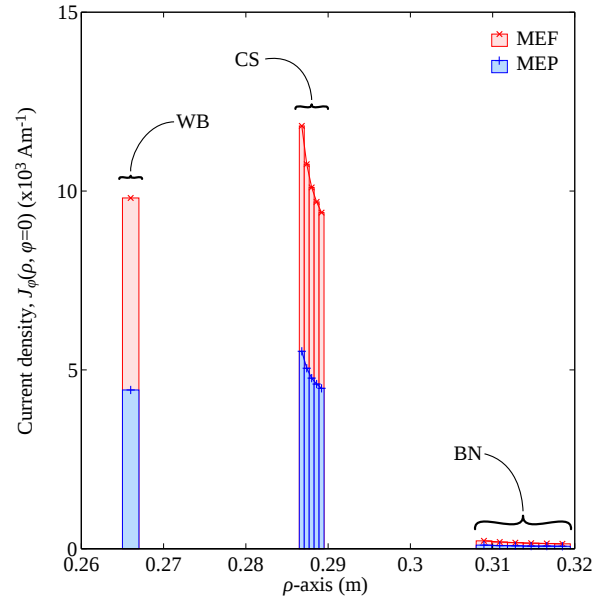


Fig. 4. Root-mean-squared (RMS) current density, $J_\phi(\rho, \phi = 0)$, for each sub-layer of the magnet cryostat and support structures

Similarly, the sum-of-squares of the current density was calculated in the ρ -direction for each layer to obtain the total current density in the WB, CS and BN. Data for the MEF and MEP gradient coils are shown separately in Figs. 5 a) and b) respectively. The amount of eddy current in the CS is slightly less than that in the WB and the amount induced in the BN is approximately 20 times smaller than that in the WB.

2) *Total Power*: The total amount of power that is dissipated in each layer for each gradient coil was computed and appears in Table III. This gives a comparative simulated measure of the amount of heating that occurs in each layer and is indicative of the vibration power imparted to the layer.

TABLE III
AMOUNT OF POWER DISSIPATED IN WATTS (W) BY EACH LAYER FOR THE TWO DIFFERENT TYPES OF GRADIENT COILS GENERATING A 10 MTm^{-1} GRADIENT FIELD OSCILLATING AT 1 KHZ

Layer name	Warm bore	Cold shield	Bobbin
Min Eddy Field	26.75	3.79	0.05
Min Eddy Power	6.10	0.98	0.01

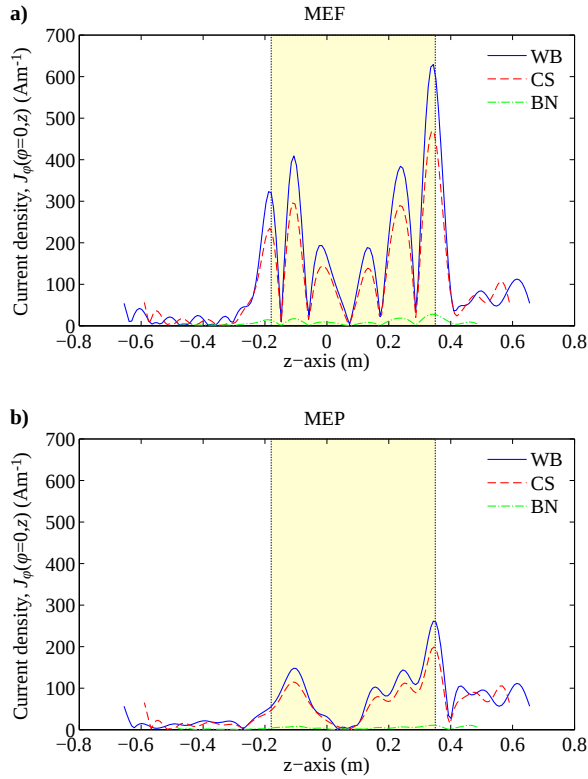


Fig. 5. Square-root of the sum-of-squares current density, $J_\phi(\rho, \phi = 0)$, for each layer of the magnet cryostat and support structures for a) the minimum eddy field and b) eddy power coils. Vertical dotted lines indicate the axial extents of the gradient coils.

3) *Eddy Current Magnetic Field*: The magnetic field generated by the eddy currents, B_{Ez} , in the ROI for both types of gradient coil shielding is shown in Fig. 6. The field is calculated across the ROI in the x -direction for $y = z = 0$ and has the same $\cos \phi$ variation as the eddy currents. The gradient field at the origin is 0.07 and 0.11 mTm^{-1} for the minimum eddy field and power coils respectively, which represents 0.7% and 1.1% of the intended gradient field.

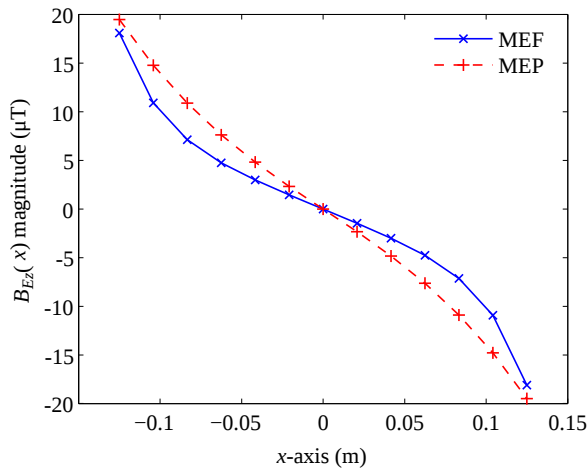


Fig. 6. Total magnetic field magnitude generated by the eddy currents induced by both the MEF and MEP coils in the ROI.

IV. DISCUSSION

The approach to gradient coil simulation used in the present study allows us to predict the eddy currents generated from any type of coil. Previous methods have been restricted to zonal coils; that is, those that have no ϕ variation of $\mathbf{J}_E(\mathbf{r})$ and are made of co-axial, circular loops [11], [12]. Although not presented in this work we may simulate Y and Z gradient coils, as well as shim and other coils. We are limited in the present method to simulation of eddy currents on any number of cylinders of finite length with any thickness and electromagnetic property. Also, in the present study we considered only those eddy currents that have a current density with $\cos(m\phi)$ variation where $m = 1$; The method is not restricted to the use of a single value of m but may be performed for $m = 0, 1, 2, \dots, M$ (including $\sin(m\phi)$ variations), but calculation time will increase as a consequence.

The eddy current layers simulated in the model presented in this work have different temperatures, material properties and thicknesses. It was found that using 12 sub-layers (so that each sublayer was less than $1/5^{\text{th}}$ of the skin-depth of that layer) to model the 3 thick cylinders provided less than 1% error with respect to result obtained with 24 layers. Figure 4 shows the skin effect through the thickness of each layer, which is prominent in the CS, less pronounced in the BN and negligible in the WB. For simulation of truly superconducting material, only thin shell on the ID of the layer would need to be considered - which is the approximation used in the design of shielding for gradient coils. Furthermore, it was found that 28 truncated sinusoids were needed in each layer to provide a calculation error of less than 1%. This represents a maximum spatial frequency of 78 mm^{-1} for the simulated eddy currents.

Simulation of thick cylinders using this network method approach was shown previously to be valid for cylinders that may be thick with respect to the skin depth but are thin compared to the other dimensions of the cylinder; i.e. the length and radius of the cylinder is much larger than its thickness. The model system used for this study does not include the full cryostat but just the cylindrical bore tube. The validity of omitting the cryostat end flanges rests on the assumption that the eddy currents are small at the ends of the cylinders, which is corroborated by the data shown in Fig. 5. Furthermore, inclusion of the full geometry of the bobbin is not possible as it is significantly different in shape to a cylinder where material surrounds and supports the superconductors. The full shape is not modelled, but the bobbin is included to give an idea of the order of magnitude of the eddy currents present in the bobbin, which appear to be small and have negligible effect on the magnetic field and only a small amount of dissipation occurs in the bobbin.

From Fig. 2 it can be seen that the primary coils of both different types of gradient coil are very similar. However, the shields appear to be quite different. This comes from the way in which the shielding is incorporated into the design functional, Eq. (1) and results in different eddy currents induced in the WB, CS and BN. Shielding by Eq. (2) only indirectly penalises currents flowing in the magnet cryostat, whereas Eq. (3) directly minimises the sum-of-squares of the

eddy current density. The effect is clear from Fig. 5: the eddy currents induced by the gradient coil in Fig. 2 a) are highly-oscillatory and have a high peak value whereas, with the coil in Fig. 2 b), the eddy currents are more smooth in z and have lower peak amplitude. This effect in turn causes the power dissipation in each layer of the magnet cryostat to be 4.4 (WB), 3.9 (CS) and 3.6 (BN) times as small in the case where the power in the cryostat was minimised. The current density in the CS was found to be similar to that which flows in the WB, but because of its low resistivity, the currents remain for a long time and are not dissipated leading to approximately 6-7 times more power dissipated in the WB than the CS.

The magnetic fields generated by the eddy currents of both types of gradient coil were simulated in the ROI along a line in x through the origin. It was expected that the field produced by the MEF coil be much less than that of the MEP coil. In our simulated data, the gradient field at the origin was 0.7% and 1.1% of the primary field for the MEF and MEP coils respectively. It is thought that the similarity between these values is related to the discretisation of the stream function into the wires of the coil design. The coils presented in this study are based on real designs and engineering constraints that dictated the use of 8 and 7 stream function contours. No study of the effect of changing the number of wires used to make the gradient coil was made, but it is suspected by the authors that the eddy current field will reduce for the MEF coil as the number of contours increases.

The MEF and MEP shielding terms (Eqs (2) and (3)) are both quadratic with respect to the solutions and Eq. (1) is solved by matrix inversion. It is possible to use a weighted sum of the MEF and MEP shielding terms in Eq. (1), but this trade-off was not investigated in the present study.

V. CONCLUSION

A high-temperature superconducting MRI scanner for human head imaging was simulated with respect to eddy currents generated by the X gradient coils. A recently proposed network simulation method for thick cylinders was used with spectral decomposition of the current density in the z and ϕ directions and multiple thin layers in the ρ direction. Previous methods of simulating eddy currents induced by gradient coils in MRI have been limited to coils that are composed of coaxial circular loops of wire. These simulations will inform the design of gradient coils for this novel system which is expected to be sensitive to electromagnetic and mechanical disturbances from the gradient coils.

Two types of gradient coil shielding were evaluated; one in which the magnetic field from the eddy currents was minimised (MEF) and another in which the power dissipated by the eddy currents is minimised (MEP). A much lower power dissipation was simulated in the case of the MEP coil, as expected. However, only a slight reduction in the eddy current induced magnetic field was seen for the MEF coil.

ACKNOWLEDGMENT

This work was funded by the MedTeQ Centre of Queensland and JST-SENTEN, System Development Program for Advanced Measurement and Analysis.

REFERENCES

- [1] R. Turner, "Gradient coil design: A review of methods," *Magnetic Resonance Imaging*, vol. 11, no. 7, pp. 903–920, 1993.
- [2] P. C. Lauterbur, "Image formation by induced local interactions: Examples employing nuclear magnetic-resonance," *Nature*, vol. 242, no. 5394, pp. 190–191, 1973.
- [3] A. N. Garroway, P. K. Grannell, and P. Mansfield, "Image formation in NMR by a selective irradiative process," *Journal of Physics C: Solid State Physics*, vol. 7, no. 24, pp. L457–L462, 1974. [Online]. Available: <http://stacks.iop.org/0022-3719/7/L457>
- [4] R. Turner and R. M. Bowley, "Passive screening of switched magnetic field gradients," *Journal of Physics E: Scientific Instruments*, vol. 19, no. 10, pp. 876–879, 1986. [Online]. Available: <http://stacks.iop.org/0022-3735/19/876>
- [5] D. C. Flugan, "Nuclear magnetic resonance eddy current field suppression apparatus," US Patent 4,585,955, 1986.
- [6] M. Morich, D. A. Lampman, W. Dannels, and F. T. D. Goldie, "Exact temporal eddy current compensation in magnetic resonance imaging systems," *IEEE Transactions on Medical Imaging*, vol. 7, no. 3, pp. 247–254, 1988.
- [7] P. Mansfield and B. Chapman, "Active magnetic screening of gradient coils in nmr imaging," *Journal of Magnetic Resonance*, vol. 66, no. 3, pp. 573–576, Feb. 1986.
- [8] G. N. Peeren, "Stream function approach for determining optimal surface currents," *Journal of Computational Physics*, vol. 191, no. 1, pp. 305–321, Oct. 2003. [Online]. Available: <http://www.sciencedirect.com/science/article/B6WHY-49CSWYW-1/2/8f2dfa499ec1e4fa64c7e5cdcd02b7f6>
- [9] R. Brown, Y. Cheng, T. Eagan, T. Kidane, H. Mathur, R. Petschek, W. Sherwin, S. Shvartsman, and J. Willig, "Toward shielding improvements in mri gradients and other systems," *Magnetic Resonance Materials in Physics, Biology and Medicine*, vol. 13, no. 3, pp. 186–192, Oct. 2001. [Online]. Available: <http://dx.doi.org/10.1007/BF02678595>
- [10] H. Sanchez Lopez, M. Poole, and S. Crozier, "Eddy current simulation in thick cylinders of finite length induced by coils of arbitrary geometry," *Journal of Magnetic Resonance*, vol. 207, pp. 251–261, 2010.
- [11] W. A. Edelstein, S.-A. E. Hamamsy, J. F. Schenck, W. D. Barber, and D. A. Gross, "Calculation of time-dependent, gradient-induced axisymmetric eddy currents and fields," in *Proceedings of the International Society for Magnetic Resonance in Medicine*, vol. 5, 1997, p. 1661.
- [12] A. Trakic, F. Liu, H. S. Lopez, H. Wang, and S. Crozier, "Longitudinal gradient coil optimization in the presence of transient eddy currents," *Magnetic Resonance in Medicine*, vol. 57, no. 6, pp. 1119–1130, 2007. [Online]. Available: <http://dx.doi.org/10.1002/mrm.21243>
- [13] W. A. Edelstein, T. K. Kidane, V. Taracila, T. N. Baig, T. P. Eagan, Y.-C. N. Cheng, R. W. Brown, and J. A. Mallick, "Active-passive gradient shielding for mri acoustic noise reduction," *Magnetic Resonance in Medicine*, vol. 53, no. 5, pp. 1013–1017, 2005. [Online]. Available: <http://dx.doi.org/10.1002/mrm.20472>
- [14] J. D. Jackson, *Classical Electrodynamics, 3rd Edition*. John Wiley and Sons, Ltd., 1998.
- [15] Z. J. J. Stekly, "Continuous, transverse gradient coils with high gradient uniformity," in *Proceedings of the Society for Magnetic Resonance in Medicine*, vol. 4, 1985, p. 1121.
- [16] J. W. Carlson, K. A. Derby, K. C. Hawryszko, and M. Weideman, "Design and evaluation of shielded gradient coils," *Magnetic Resonance in Medicine*, vol. 26, no. 2, pp. 191–206, 1992. [Online]. Available: <http://dx.doi.org/10.1002/mrm.1910260202>
- [17] G. N. Peeren, "Stream function approach for determining optimal surface currents," Ph.D. dissertation, Technische Universiteit Eindhoven, 2003.
- [18] M. Poole and R. Bowtell, "Azimuthally symmetric ibem gradient and shim coil design," in *Proceedings of the International Society for Magnetic Resonance in Medicine*, vol. 16, 2008, p. 345.
- [19] D. C. Alsop and T. J. Connick, "Optimization of torque-balanced asymmetric head gradient coils," *Magnetic Resonance in Medicine*, vol. 35, no. 6, pp. 875–886, 1996. [Online]. Available: <http://dx.doi.org/10.1002/mrm.1910350614>
- [20] M. A. Brideson, L. K. Forbes, and S. Crozier, "Winding patterns for actively shielded shim coils with asymmetric target-fields," *Measurement Science and Technology*, vol. 14, no. 4, pp. 484–493, Apr. 2003.
- [21] S. Pissanetzky, "Minimum energy mri gradient coils of general geometry," *Measurement Science and Technology*, vol. 3, no. 7, pp. 667–673, 1992. [Online]. Available: <http://stacks.iop.org/0957-0233/3/667>

- [22] M. Poole and R. Bowtell, "Novel gradient coils designed using a boundary element method," *Concepts in Magnetic Resonance Part B: Magnetic Resonance Engineering*, vol. 31B, pp. 162–175, 2007.